

Moving Particle Simulation for Mitigation of Sloshing Impact Loads Using Surface Floaters

B.-H. Lee¹, J.-C. Park², M.-H. Kim³ and S.-C. Hwang²

Abstract: The violent free-surface motions and the corresponding impact loads are numerically simulated by using the refined Moving Particle Simulation (MPS) method, which was originally proposed by Koshizuka and Oka (1996) for incompressible flows. In the present method, accuracy and efficiency are significantly improved compared to the original MPS method by using optimal source term, optimal gradient and collision models, and improved solid-boundary treatment and search of free-surface particles. The refined MPS method was verified through comparisons against Kishev et al.'s (2006) sloshing experiment. It is also demonstrated that the refined MPS method is excellent in mass conservation regardless of length of simulation time. The developed simulation tool is applied to an interesting idea of using surface floaters to reduce sloshing-induced impact loads. It is seen by a series of simulations that the maximum impact loads can be effectively reduced by using properly chosen floater density.

Keywords: Mitigation of sloshing impact loads, Moving Particle Simulation (MPS), Surface floaters, Long-time simulation, Navier-Stokes equation

1 Introduction

Recently, the order of super-size LNG (Liquefied Natural Gas) carrier, LNG-FPSO (Floating Production Storage and Offloading), and LNG FSRU (Floating Storage Re-gasification Unit) has been increased considering the economics of business and operation. As a result, there is much higher probability of navigation and operation with partially-filled liquid cargos. When fluid is partially filled in liquid cargo tanks, internal impact loads can occur inside the tank by vessel motions, called

¹ Department of Ocean Industry Research, Hyundai Maritime Research Institute, Ulsan, Korea

² Naval Architecture and Ocean Engineering Department, Pusan National University, 30 Jangjeondong, Geumjeong-gu, Busan, Korea, Tel.: +82-51-510-2480, Fax.: +82-51-583-2485, E-mail: jcpark@pnu.edu

³ Dept. of Civil Engineering, Texas A&M University, USA

“sloshing”. In particular, if the period of tank motion is close to the natural period of fluid-sloshing, it causes violent liquid motions and large structural loads. Especially, the possible structural damage and leak of LNG tank wall under very violent sloshing and very brittle condition at -163°C is a big concern since it can lead to more serious accidents. Therefore, the understanding of the physics of sloshing phenomena and the reliable prediction of sloshing loads are important elements in the design procedure of such structures. Until now, many researchers have investigated the sloshing problem by using physical and numerical modeling. Various numerical simulation methods have been applied and the accurate prediction of sloshing-induced impact loads is still considered to be very challenging.

The numerical treatment of this kind of highly nonlinear free-surface behavior is usually very difficult due to the complexity associated with fully-nonlinear free-surface and body- boundary conditions. In particular, how to trace free-surface particles in case of very violent motions, such as overturning, plunging, overshooting, and splashing, is the most challenging task. There are several CFD techniques to handle such problems, i.e. SOLA-VOF (Hirt and Nichols (1981)), Level-Set (Sussman, Smereka and Osher (1994)), Marker-Density Function (MDF) (Miyata and Park (1995)) etc. Most of them are the techniques capturing the free surface on grid system. However, there is a different approach without grid system, so-called particle method by use of kernel function and Lagrangian treatment of particles. For example, Koshizuka and Oka (1996), Sueyoshi and Naito (2003), Lee, Park, Kim and Hwang (2011) and Gotoh (2009) developed MPS (Moving Particle Simulation) method, while Gingold and Monaghan (1977), Monaghan (1988) and Dalrymple and Rogers (2006) used SPH (Smoothed Particle Hydrodynamics). Also, Idelsohn, Onate and Del Pin (2004) developed PFEM (Particle Finite Element Method) for incompressible flows with breaking waves. In the MPS method, kernel-function-based difference algorithms are used for differentiation. On the other hand, kernel functions are directly differentiated in the SPH method. It is well known that there are pros and cons in both MPS and SPH methods compared to each other.

For certain problems including complicated boundary shapes/conditions or fluid/structure coupling, the particle methods may be more reliable and effective than conventional grid methods. The MPS method was originally proposed by Koshizuka and Oka (2006) for incompressible flow. In the MPS method, the convection terms in Navier–Stokes equation can be more directly treated without numerical diffusion and instabilities. The method consists of the particle interaction models representing gradient, diffusion, incompressibility, and the boundary conditions. In the original MPS method, however, there were several defects including non-optimal source term, non-optimal gradient and collision models, and non-optimal search of free-surface particles, which led to more computational time, less-accurate fluid

motions, and non-physical pressure fluctuations, as pointed out and modified by Khayyer and Gotoh (2009; 2011), Lee, Park, Kim and Hwang (2011).

In the present study, we briefly illustrate the revised MPS method by), Lee, Park, Kim and Hwang (2011). As an example, we first consider liquid sloshing inside a rectangular tank under forced oscillation and the simulation results are compared against Kischev, Hu and Kashiwagi (2006)'s experiment. The comparison shows that the refined MPS method correlates well with the experimental data. After this validation, the refined MPS method is further applied to the same sloshing problem with a thin top layer of particles of different density to observe their effects on the maximum impact loading (Hwang, Lee, Park and Sung, 2010; Kim, Kim, Kim, Jeon, Seo, Park, Hwang-Bo and Lee, 2011). It is shown that the top layer with light density may be effective in reducing the maximum impact loads on the wall under the same forced oscillation. Since the employed scheme is very stable and the conservation of mass is accurately satisfied in the present method, we can simulate the violent liquid sloshing motions for a very long time to more meaningfully find, for example, the stochastically maximum sloshing-induced impact loads. For such a long simulation with a large number of particles, computational time efficiency is very important, which is one of the merits of the present method. In this paper, the examples are limited to 2D problems but the same schemes and principles would be directly applicable to 3D problems.

2 Moving Particle Simulation (MPS) Method

2.1 Governing Equations

The Governing equations for incompressible viscous flows are the continuity and Navier-Stokes equations as follows:

$$\frac{D\rho}{Dt} = 0 \quad (1)$$

$$\frac{D\vec{u}}{Dt} = -\frac{1}{\rho}\nabla P + \nu\nabla^2\vec{u} + \vec{F} \quad (2)$$

The symbol ρ is the density, t the time, \vec{u} the velocity vector, ∇ the gradient, P the pressure, ν the kinematic viscosity, and \vec{F} the external force.

The continuity equation (Eq. (1)) is written with respect to the density, while velocity divergence is usually used in grid methods. The left-hand side of Navier-Stokes equation (Eq. (2)) denotes Lagrangian differentiation including convection terms. This is directly calculated by moving particles in a Lagrangian manner. The right-hand sides consist of pressure gradient, viscous, and external-force terms. To simulate incompressible flows, all terms expressed by differential operators should

be replaced by the particle interaction models of the MPS method proposed originally by Koshizuka and Oka (1996). In the present paper, the newly developed MPS (called PNU-MPS from this point on) method (Lee, Park, Kim and Hwang (2011)) is employed for all simulation, which can calculate the flow field with violent free-surface motion more accurately and stably compare to the original MPS (Koshizuka and Oka (1996)).

2.2 Kernel Function

Continuous fluid can be represented by physical quantities of coordinates, mass, velocity components, and pressure for particles. The governing equations written with partial differential operators are transformed to the equation of particle interactions. The particle interactions in the MPS method are based on the kernel function. In this study, the following function is employed:

$$w(r) = \begin{cases} \left(1 - \frac{r}{r_e}\right)^3 \left(1 + \frac{r}{r_e}\right)^3 & (0 \leq r < r_e) \\ 0 & (r_e < r) \end{cases} \quad (3)$$

The distance between two particles is r and r_e represents the effective range of particle interactions. The kernel becomes zero where $r > r_e$. Since the area covered with this weight function is bounded, a particle interacts with a finite number of neighboring particles. The radius of the interaction area is determined by the parameter, r_e . The weighting of interaction between two particles can be described by the kernel function; i.e. the nearer the distances between two particles, the larger the weight of interactions. If the distance between two particles is quite long, their interactions can be neglected.

2.3 Gradient Model

A gradient vector between two particles i and j possessing scalar quantities φ_i and φ_j at coordinates r_i and r_j is defined as $(\varphi_j + \varphi_i)(\vec{r}_j - \vec{r}_i)/|\vec{r}_j - \vec{r}_i|^2$ based on the action-reaction physical law (Toyoda, Akimoto and Kubo (2005)). The gradient vector at the particle i is given by the weighted average of these gradient vectors:

$$\langle \nabla \varphi \rangle_i = \frac{d}{n^0} \sum_{i \neq j} \left[\frac{\varphi_j + \varphi_i}{|\vec{r}_j - \vec{r}_i|^2} (\vec{r}_j - \vec{r}_i) w(|\vec{r}_j - \vec{r}_i|) \right] \quad (4)$$

where d is the number of space dimensions and n^0 is the particle number density fixed for incompressibility of the initial condition of particle arrangement. The particle number density is calculated by the following equation.

$$n_i = \sum_{i \neq j} w(|\vec{r}_j - \vec{r}_i|) \quad (5)$$

The fluid density is proportional to the particle number density.

2.4 Laplacian Model

The diffusion of ϕ at particle i is described by

$$\nabla^2 \phi = \frac{2d}{\lambda} (\phi_j - \phi_i) w(|r_j - r_i|) \quad (6)$$

$$\lambda = \frac{\sum_{j \neq i} w(|\vec{r}_j - \vec{r}_i|) |r_j - r_i|^2}{\sum_{j \neq i} w(|\vec{r}_j - \vec{r}_i|)} \cong \frac{\int_V w(r) r^2 dv}{\int_V w(r) dv} \quad (7)$$

where λ is the parameter by which the variance increase is equal to that of the analytical solution.

2.5 Incompressibility Model

Fluid density is represented by the particle number density. Thus, the continuity equation (1) is fulfilled with fixing the particle number density through the simulation. This means that the particle number density n^0 should be constant.

The algorithm of incompressibility for the PNU-MPS method is similar to that of the SMAC (Simplified Marker-and-Cell) method in grid system. In each time step, there are two stages: in the first stage, the temporal velocity components \vec{u}_i^* of particle i is obtained using viscous terms, external forces, and convection terms, which are explicitly calculated with the values \vec{u}_i^n and \vec{r}_i^n in the (n)-th time step.

In the second stage, the Poisson equation for pressure is calculated implicitly:

$$\nabla^2 P_i^{n+1} = (1 - \gamma) \frac{\rho}{\Delta t} \nabla \cdot \vec{u}_i^* + \gamma \frac{\rho}{\Delta t^2} \frac{n^0 - n_i^n}{n^0} \quad (8)$$

The blending parameter γ of the right-hand side of Eq. (8) is less than 1.0 and the range of $0.01 < \gamma < 0.05$ is recommended in Lee et al. (2011).

The left-hand side of Eq. (8) is discretized by the Laplacian model of Eq. (6). The first source term of Eq. (8) is the divergence-free condition and calculated by the following equation:

$$\langle \nabla \cdot \vec{u} \rangle_i = \frac{d}{n^0} \sum_{i \neq j} \frac{(\vec{u}_j - \vec{u}_i) \cdot (\vec{r}_j - \vec{r}_i)}{|\vec{r}_j - \vec{r}_i|^2} w(|r_j - r_i|) \quad (9)$$

And the second source term of Eq. (8) is represented by the deviation of the particle number density from the constant and means that the particle number densities should be maintained during the simulation.

In Eq. (8), we have simultaneous equations expressed by a linear symmetric matrix and they are solved by iteration method. In the present study, the CG (Conjugate Gradient) method is employed as the iterative solver.

After updating the pressure field, the velocity correction \vec{u}'_i is calculated by the following equation:

$$\vec{u}'_i = -\frac{\Delta t}{\rho} \langle \nabla P_i^{n+1} \rangle \quad (10)$$

Finally, the velocity components and coordinates of particles in the $(n + 1)$ -th time step are calculated from the following equations:

$$\vec{u}_i^{n+1} = \vec{u}_i^* + \vec{u}'_i \quad (11)$$

$$\vec{r}_i^{n+1} = \vec{r}_i^n + \Delta t \vec{u}_i^{n+1} \quad (12)$$

The computational procedure for PNU-MPS method is shown in **Fig. 1**.

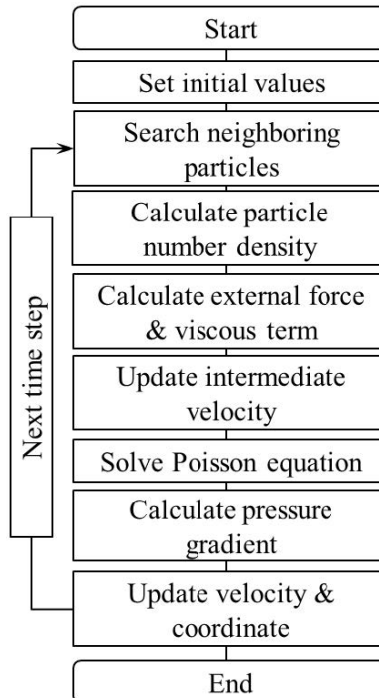


Figure 1: Computational procedure of PNU-MPS.

2.6 Boundary Condition

As the free-surface boundary condition, the kinematic and dynamic boundary conditions are imposed. The kinematic boundary condition can be directly satisfied by moving particles on the free-surface. In the present method, it is straightforward to track the free-surface particles because the location of the free-surface is easily obtained as a result of the fully Lagrangian treatment of particles.

In the vicinity of the free-surface, the particle number densities are decreased due to the comprisal of the air region, where no particles exist in case of single-phase problem. Thus, on the free surface, the particles satisfying the following conditions are considered:

$$\langle n \rangle_i^n < \beta_1 n^0 \quad (13)$$

$$N_i < \beta_2 N^0 \quad (14)$$

where β_1 and β_2 are parameters below 1.0, N_i the number of neighboring particles within effective range of particle interaction r_e , and N_0 the maximum number of neighboring particles for fully submerged particles in the initial distribution. Especially, the free-surface parameter β s are used to judge whether the particles are on the free-surface or not, and β_1 and β_2 are set at 0.97 and 0.85 respectively in this study, which are based on the results from the independently performed numerical experiments. Using this free-surface boundary condition, the simulation of fragmentation and coalescence of free-surface flow is available.

Assuming that there is no viscosity at the free-surface, the dynamic free-surface boundary condition is satisfied by taking the atmosphere pressure ($P = P_{atm} = 0$) on the free-surface particles. This condition is fulfilled in the procedure of solving the Poisson equation (8). In the present study, only one-phase (liquid only) is used and air particles are not separately employed.

As for wall boundary condition, it is not easy to satisfy the velocity boundary condition on wall due to the movement of fluid particles at each step. In particle method, it is important to get the useful information of physical quantities from the neighboring particles. The physical quantities are calculated through interaction with those of neighboring particles. The wall particles are directly in contact with both the fluid and dummy particles. They are involved in the pressure calculation and prevent the concentration of particles near the wall. In this study, we introduce moving dummy particles. The dummy particles corresponding to the fluid particle with normal to the wall are rearranged inside the wall at each time step, as shown in **Fig. 2**. Then, the pressure for dummy particles is extrapolated by consideration of the static pressure from the corresponding fluid particles, and the velocities

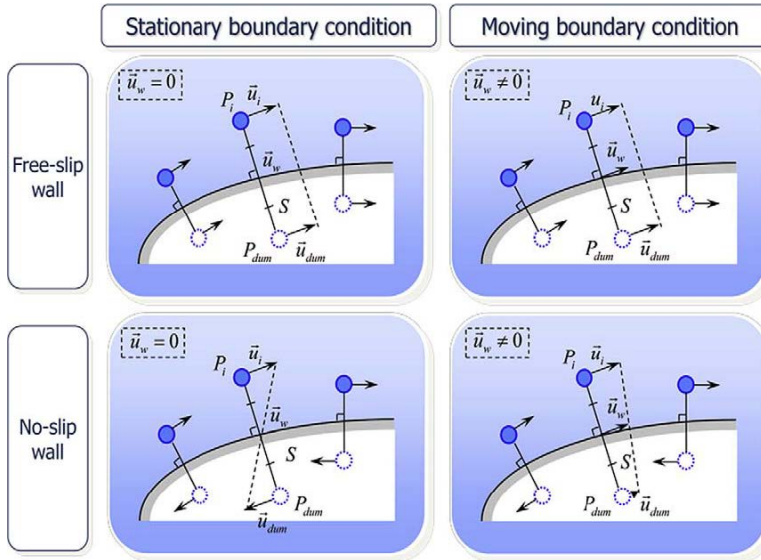


Figure 2: Description of velocity boundary condition for dummy particles, where the hollow circles indicate dummy particles.

for dummy particles are treated either free-slip or no-slip condition by following manners:

i) free-slip condition

$$P_{dum} = P_i + \rho gh, \quad \vec{u}_{dum} \cdot \vec{n} = (2\vec{u}_w - \vec{u}_i) \cdot \vec{n}, \quad \vec{u}_{dum} \cdot \vec{t} = \vec{u}_i \cdot \vec{t}$$

ii) no-slip condition

$$P_{dum} = P_i + \rho gh, \quad \vec{u}_{dum} \cdot \vec{n} = (2\vec{u}_w - \vec{u}_i) \cdot \vec{n}, \quad \vec{u}_{dum} \cdot \vec{t} = (2\vec{u}_w - \vec{u}_i) \cdot \vec{t}$$

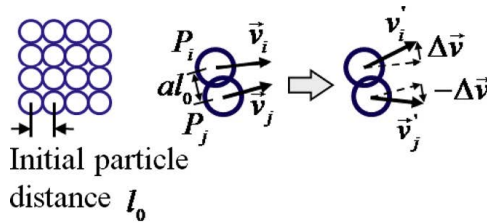
where h is the vertical distance from the corresponding fluid particle, \vec{n} and \vec{t} are the normal and tangential vectors to the wall, and the subscripts for dum, i and w indicate the dummy, corresponding fluid and wall particles, respectively.

In the present study, the no-slip condition on wall is imposed for all simulations. And three layers of particles are located to ensure that the particle number density is computed accurately.

2.7 Collision model

When particles get close inside fluid, repulsive force due to the local pressure can be calculated without introducing any special collision model. For the particles on the free surface, however, the pressure is fixed by the constant atmospheric pressure, and thus, repulsive forces are not properly generated even when particles get close. In particular, when the particles accelerated from outside collide with free surface, the particle number density can suddenly be increased. As a result, it may not be recognized as a free-surface particle, so the pressure can be suddenly increased. This phenomenon greatly reduces the spatial stability of the pressure. Therefore, a special collision model needs to be employed to better represent the proper repulsive forces especially near the free surface.

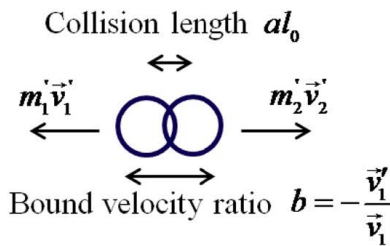
Fig. 3 shows a simple diagram for the collision model. In the beginning, the



(a) Schematic diagram



(b) Before collision



(c) At the collision moment

Figure 3: Diagram of collision model.

particles are uniformly distributed with constant distance of l_0 . When the distance between any two particles gets smaller than al_0 , the collision model is applied. Then, from the conservation of momentum, the repulsive velocity can be calculated by using the coefficient b , which is defined as the ratio of $b = -\vec{v}'/\vec{v}$. The range of good performance of $a>0.85$ and $b<0.2$ is recommended in Lee, Park, Kim and Hwang (2011).

3 Numerical Illustrations

3.1 Validation for prediction of impact pressure by sloshing

We consider the water sloshing problem inside a 2D rectangular tank driven by a harmonic oscillator. The simulation results are compared with the experimental results of Kishev, Hu and Kashiwagi (2006). The experimental set-up is shown in **Fig. 4**. The tank width and height are 0.6 (m) and 0.3 (m), respectively. The water depth is 0.12 (m), thus the filling ratio in the tank is 40%. The tank is forced to move sinusoidally in the horizontal direction as follows:

$$X_H = A \sin(2\pi/Tt) \tag{15}$$

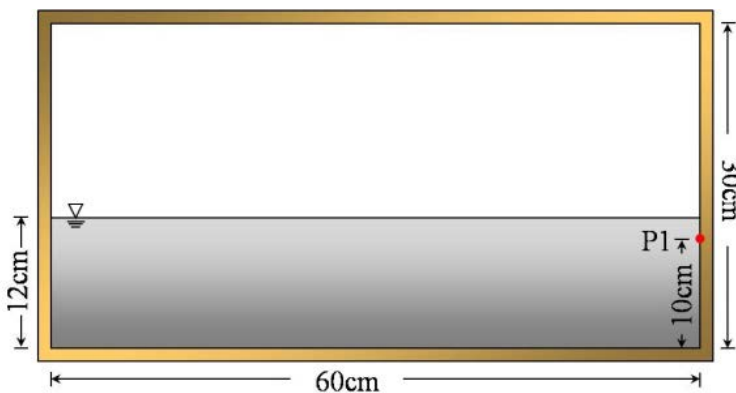


Figure 4: Schematic view of tank with dimensional and principal pressure gauge position is indicated (filling ratio=40%).

where the oscillation amplitude $A=0.05$ (m) and the periods $T=1.3$ and 1.5 (s). According to the linear potential theory (Lamb (1932)) given in Eq. (16), the natural period for the lowest sloshing mode is 1.17 (s). Being closer to the lowest natural period, the impact pressure for $T = 1.3$ (s) is expected to be larger than that of $T =$

1.5 (s).

$$T_n = \frac{2\pi}{\sqrt{\frac{\pi}{L}g \tanh\left(\frac{\pi H}{L}\right)}} \quad (16)$$

Here, H and L are the filling height and the length of the rectangular tank respectively.

The total number of particles used for the present simulation is about 4000, among which fluid particles are about 3000. The gravitational acceleration and water density are set at $9.81 \text{ (m/s}^2\text{)}$ and $1000 \text{ (kg/m}^3\text{)}$ and the surface tension is neglected. The kinematic viscosity of water is given by $\nu=10^{-6} \text{ (m}^2\text{/s)}$ and the total computational time is 16.0 (s). For the time increment in this paper, it is automatically determined according to Courant's stability condition. The collision-model coefficients a and b used for this simulation are 0.9 and 0.2. To compare with the pressure measurement of Kishev, Hu and Kashiwagi (2006), the reference point P1 on the right-side wall is selected, as shown in **Fig. 4**.

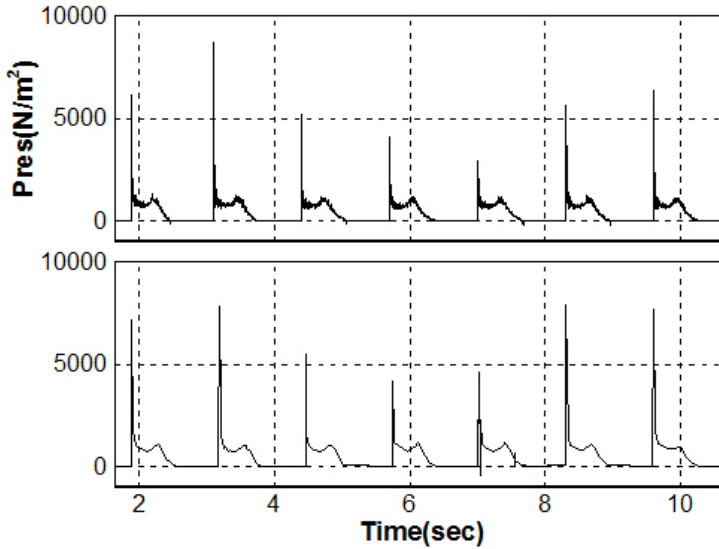


Figure 5: Comparison of sloshing-induced impact pressure profiles (top=PNU-MPS and bottom=experiment of Kishev et al. (2006): $T=1.3$ (s)).

Fig. 5 shows the comparison between experimental and simulated pressure time histories at P1 for $T=1.3$ (s). The primary peaks are caused by the initial water slamming onto the vertical wall, while the small secondary peaks are due to the fall

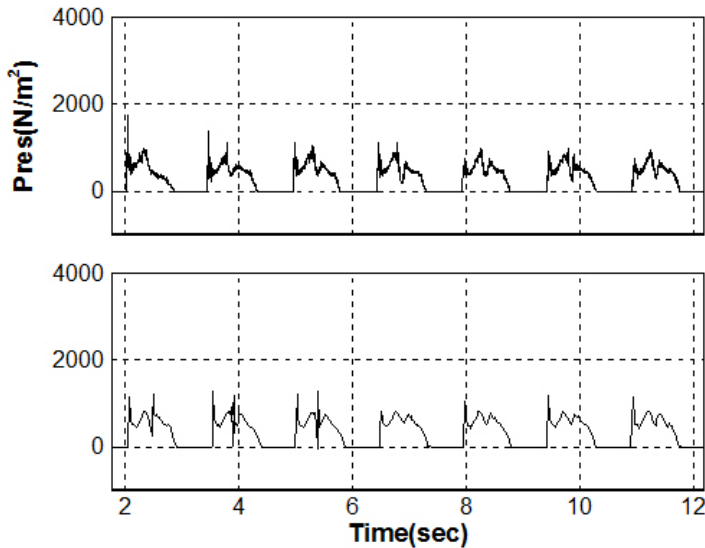


Figure 6: Comparison of sloshing-induced impact pressure profiles (top=PNU-MPS and bottom=experiment of Kishev et al. (2006): $T=1.5(\text{sec})$).

of water splash along the wall. The trend of the pressure signal between experiment and simulation is very similar.

Fig. 6 shows similar comparisons of pressure time histories in case of $T=1.5$ (s). The trend of pressure signals is different from that of **Fig. 5** since standing wave motions are overlapped with small bore motions, which results in relatively gentle initial impact, as can be more clearly seen in the snapshots given in **Fig. 7**. It is shown in Lee, Park, Kim and Hwang (2011) that the same results by using the original MPS are much worse containing physically non-existent high pressure fluctuations. Through those comparisons against experiments, it is clearly demonstrated that the present PNU-MPS method can produce very reliable liquid sloshing impact loads including very violent motions.

3.2 Prediction of stochastically meaningful impact pressure by long-time simulations

As pointed out earlier, the mass is conserved for a very long time by the present PNU-MPS method, and thus long-time simulation is possible to investigate the statistical properties of the peaks. However, it also needs to be pointed out that the sloshing experiment itself is not completely repeatable/reproducible showing different peak values at each trial. There also exists 3D effect in the experiment, so

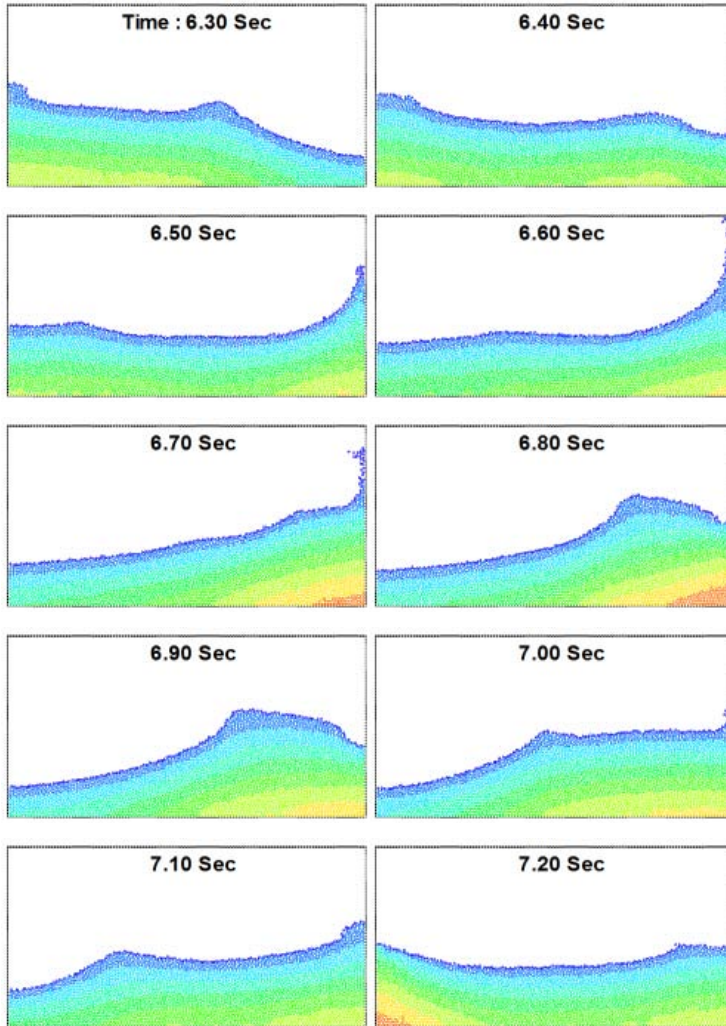


Figure 7: Snap shots of sloshing in case of $T=1.5(\text{sec})$.

perfect match against measurement is impossible.

Fig. 8 shows the initial condition for the long-time simulation of sloshing. The filling ratio in the tank is 20%. The measuring point of the pressure is P2 on the right wall. The tank is forced to move horizontally with various periods in the range of $T=0.8$ to 1.7 (s). The amplitude of the horizontal tank motion is 0.06 (m) and the total simulation time is 320 periods. Being considered as transient parts, the first 20 periods in the whole simulation results are excluded from the statistical analysis.

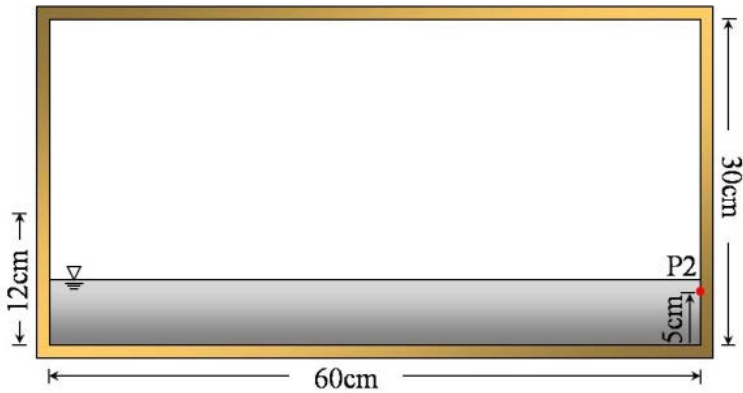


Figure 8: Schematic view of tank dimension and position of pressure gauge (filling ratio=20%).

The simulated results are compared with the experiment performed by Kishev, Hu and Kashiwagi (2006). In the experiment, three sampling times of 1, 3 and 5 (kHz) were used for the pressure measurement.

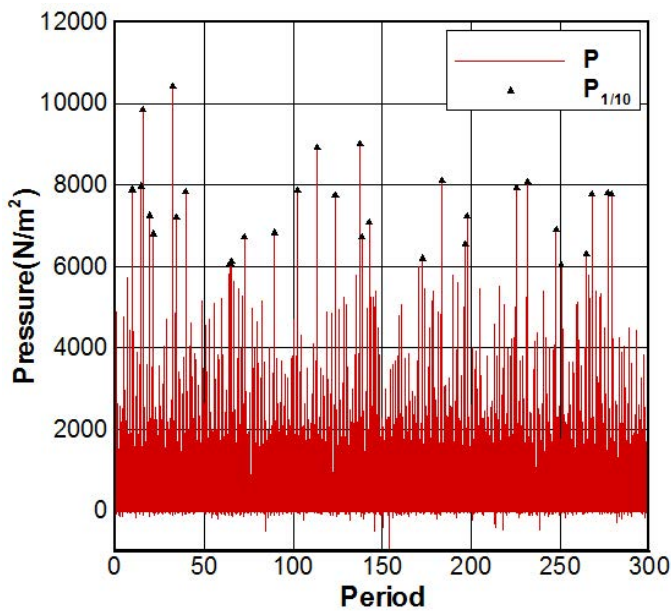


Figure 9: Time history of pressure at P2 (filling ratio=20%).

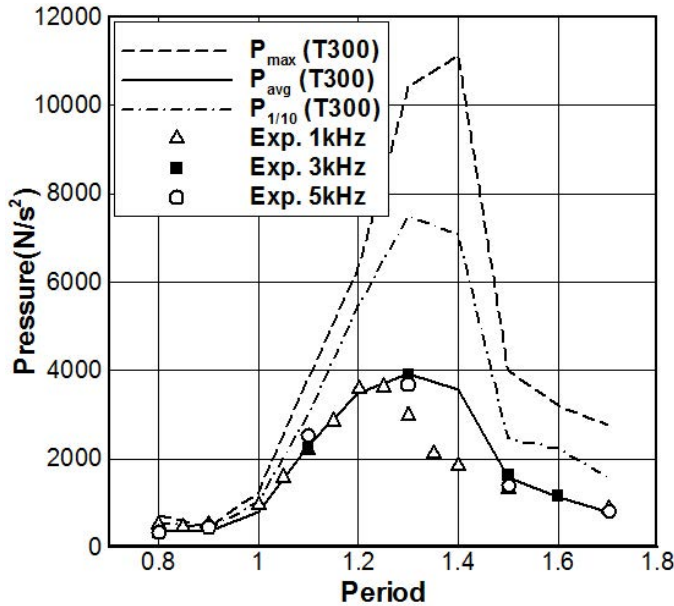


Figure 10: Peak pressure with various periods (filling ratio 20%).

Fig. 9 shows the simulated time history of the pressure acting on P2 for $T=1.3$ (s). For each period, one peak pressure is observed and its magnitude shows randomness. The symbol indicates the points used for $P_{1/10}$, average of one-tenth highest peaks, in which the 30 peak pressures belong to the top 10% among 300 peaks.

Fig. 10 shows the result of such statistical analyses with various tank-oscillation periods for the pressure acting on P2. Here, P_{max} and P_{avg} are the maximum peak value and the averaged peak value among 300 peak values. The natural frequency calculated from Eq. (16) is about 1.59 (s), while P_{max} , $P_{1/10}$, and P_{avg} have the maximum values between 1.3 and 1.4 (s). In other words, the maximum peak impact loading occurs at the oscillation period 12% smaller than the natural period predicted by the linear potential theory. That can be attributed to the significant nonlinear free-surface effects associated with violent liquid motions. The simulated averaged peak values, P_{avg} , agree well with the more reliable experimental values with higher sampling rate, as reported by Kishiev, Hu and Kashiwagi (2006).

Fig. 11 shows the sensitivity of P_{avg} and $P_{1/10}$ against the total length of simulation, 100(T100), 200(T200), and 300(T300) periods. From the results, it is seen that P_{avg} and $P_{1/10}$ values are not very sensitive to the length of simulation as long as it is more than 100 periods. The P_{max} is more sensitive than those averaged values.

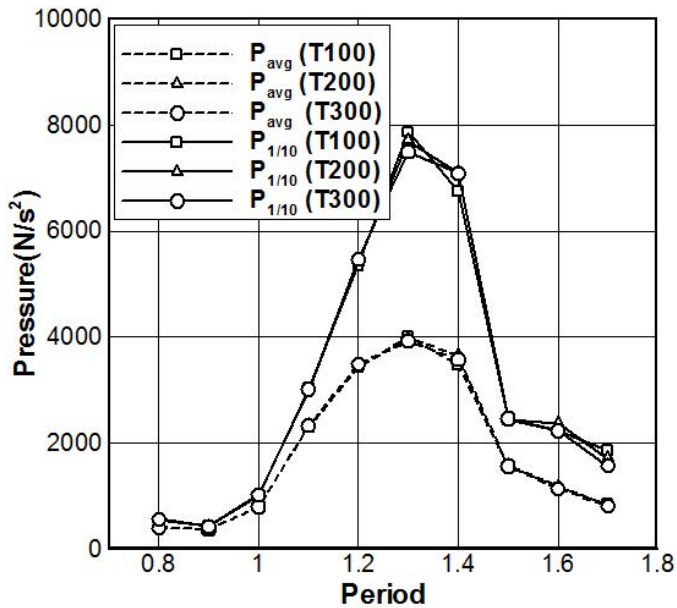


Figure 11: Averaged peak pressure with various periods.

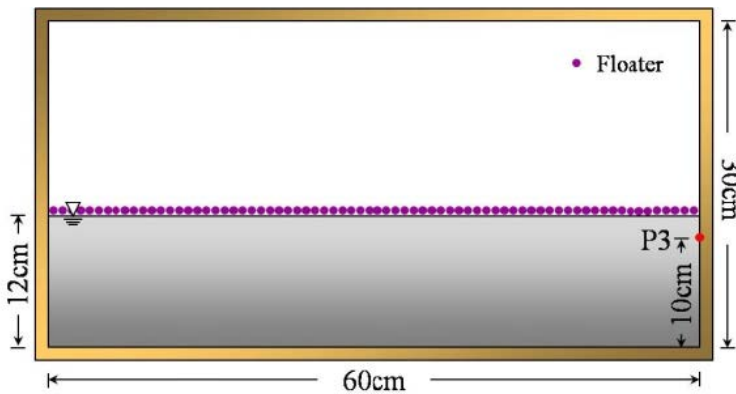


Figure 12: Initial setup for arrangement of floater over the free-surface (filling ratio=40%).

3.3 Mitigation of sloshing impact loads by using floaters

As one of the ways to mitigate the fluid impact loads by sloshing, the floaters having lighter density than water have been suggested (Hwang, Lee, Park and Sung, 2010; Kim, Kim, Kim, Jeon, Seo, Park, Hwang-Bo and Lee, 2011). To numeri-

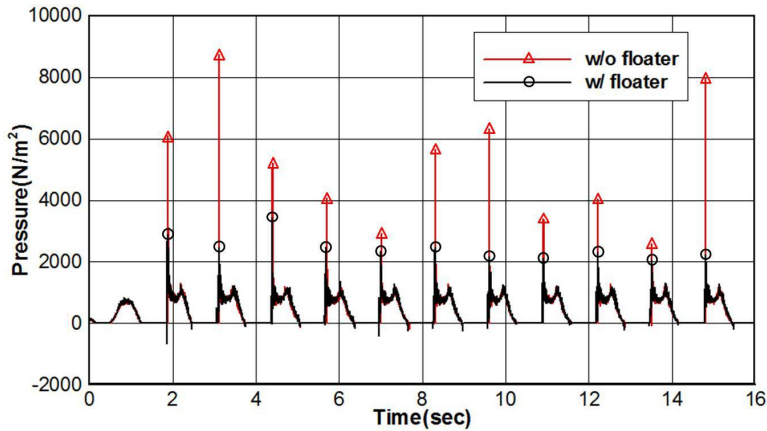


Figure 13: Comparison for time history of pressure at P3 w/ and w/o floaters ($T=1.3$ (s)).

cally demonstrate the feasibility of this idea, floater particles with light density are arranged over the free-surface as shown in **Fig. 12**. In this example, the density of the floater is set at $200 \text{ (kg/m}^3\text{)}$, while that of water particles are $1000 \text{ (kg/m}^3\text{)}$. The simulation condition is almost the same as the previous simulation described in Sec. 3.1. The initial distance between the floaters is 0.01 (m) , which is the same as that between water particles. The floaters can be regarded as thin liquid film of light density or approximately light solid floating particles. The pressure is measured at P3. The surface tension and viscosity on the free-surface are neglected. The kinematic viscosity of water is given by $\nu=10^{-6} \text{ (m}^2\text{/s)}$. The tank is forced to move horizontally according to Eq. (15). The oscillation amplitude A is 0.05 (m) and the periods are 1.3 and 1.5 (s) . For the ensuing statistical analysis, the peak pressures of 300 periods are used.

Fig. 13 shows the comparison of pressure time histories acting on P3 with and without the floaters in case of $T=1.3 \text{ (s)}$. The overall tendency looks similar between both cases, but the peak pressures with floaters are significantly decreased. From **Fig. 14**, in which free-surface snap shots are plotted for both cases, it may be reasoned why the impact pressures are reduced with floaters. During the generation of a plunging-type breaker, the floaters tend to be coalesced in front of the breaking cusp that has a relatively high acceleration, so initially contributes to the impact loading by plunging and lessens the following water impact. On the other hand, **Fig. 15** shows the case of $T=1.5 \text{ (s)}$, in which the liquid slamming on the wall is less conspicuous. As a result, the effects of floaters are less appreciable compared to the case of $T=1.3 \text{ (s)}$. The corresponding free-surface snap shots are

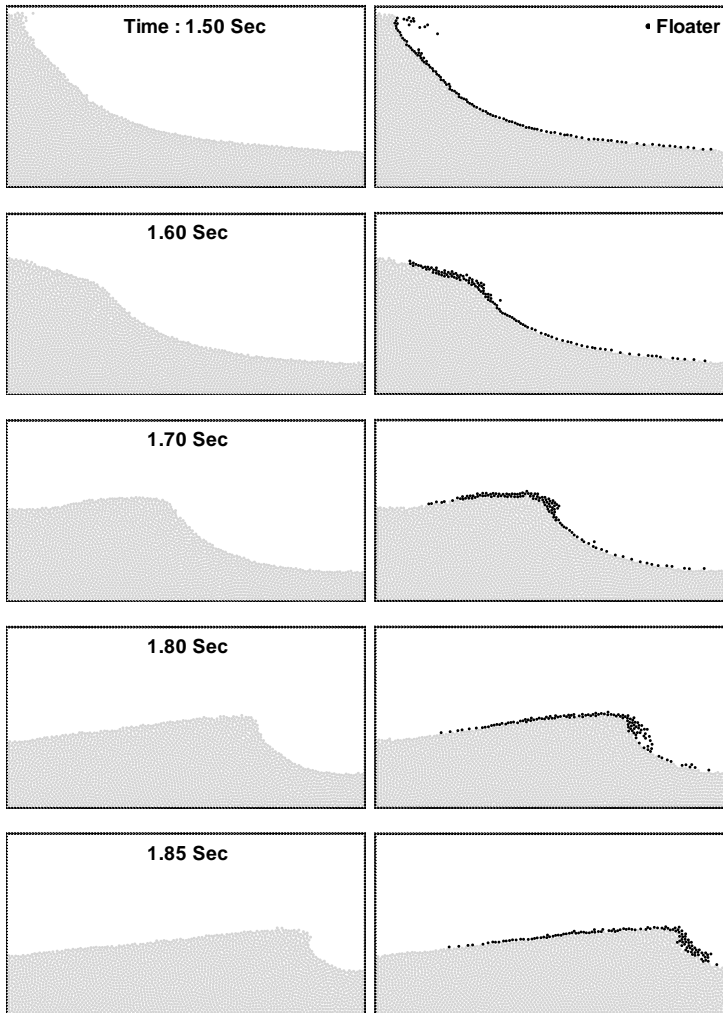


Figure 14: Time-sequential free-surface motion w/o (left) and w/ floaters (right) ($T=1.3$ (s)).

plotted in **Fig. 16** for both cases, in which relatively milder free-surface motions are observed. It means that the floaters are more efficacious for more violent sloshing cases.

Fig. 17 shows the results of a series of similar simulations for the peak pressure acting on P3 with varying floater densities. The floater density = 1000 (kg / m^3) can be considered as water only (or without floater). It is seen that if floater den-

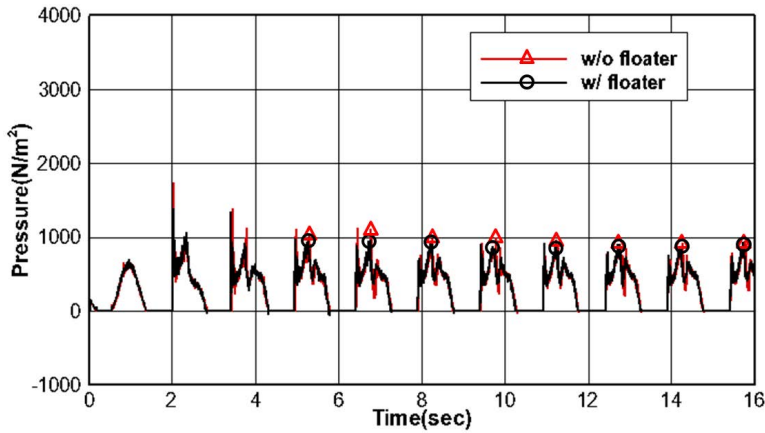


Figure 15: Comparison for time history of pressure at P2 w/ and w/o floaters ($T=1.5$ (s)).

sity is greater than $350 \text{ (kg / m}^3\text{)}$, there is no beneficial effect. The impact load is influenced by the change of momentum, so affected by both density (mass) and velocity. If the particle density is smaller, its velocity may be increased. Therefore, their combined effects may be either beneficial or detrimental and the optimal floater's density may exist. According to Fig.17, the optimal density of the floater is about $200 \text{ (kg / m}^3\text{)}$. Similar results are also given for the period 1.5 (s) in **Fig. 18**. As was seen in the previous case, the differences between with and without floaters are small since the corresponding free-surface motion is relatively mild.

Next, with fixing the floater density at $200 \text{ (kg/m}^3\text{)}$, the peak pressures are obtained for various oscillation periods with and without the floaters. **Fig. 19** and **Fig. 20** show the comparisons when the filling ratios are 40% and 20%. We can observe significant beneficial effects for both fill ratios. Especially around $T=1.3$ (s), the floaters are quite effective and about 40% reduction of $P_{1/10}$ can be observed.

4 Concluding Remarks

The violent free-surface motions and the corresponding impact loads are numerically simulated by using the Moving Particle Simulation (MPS) method, which was originally proposed by Koshizuka and Oka (1996) for incompressible flows. In the present PNU-MPS method, accuracy and efficiency are significantly improved compared to the original MPS method by using optimal source term, optimal gradient and collision models, and improved search of free-surface particles. The refined MPS method was verified through comparisons against Kishew, Hu and Kashiwagi

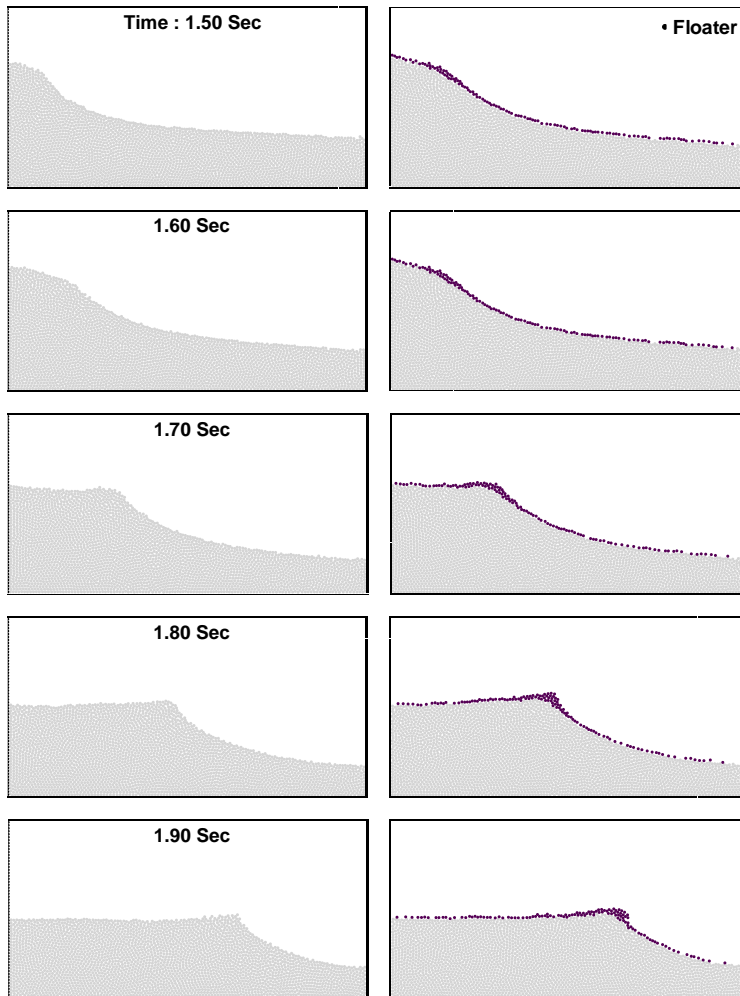


Figure 16: Time-sequential free-surface profiles w/ (left) and w/o floaters (right) (T=1.5 (s)).

(2006) sloshing experiment. Reliable pressure signals very similar to the measured ones were obtained without non-physical fluctuations. It is also demonstrated that the improved MPS method is excellent in mass conservation regardless of length of simulation time, which makes it possible to do meaningful statistical analysis with long simulation. The developed simulation tool was then applied to an interesting idea of using surface floaters to reduce sloshing-induced impact loads. It is seen that the surface floaters can be either beneficial or detrimental depending on

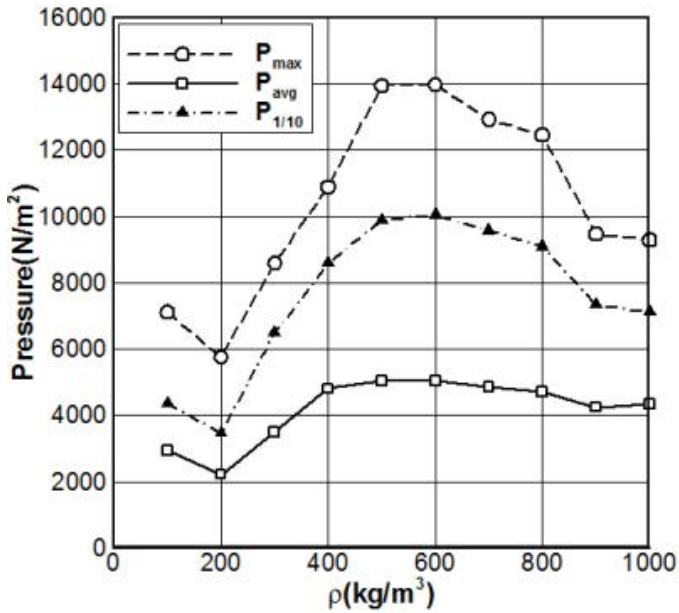


Figure 17: Results of statistical analysis for peak pressure at T=1.3 (s) with various density of floater (filling ratio=40%).

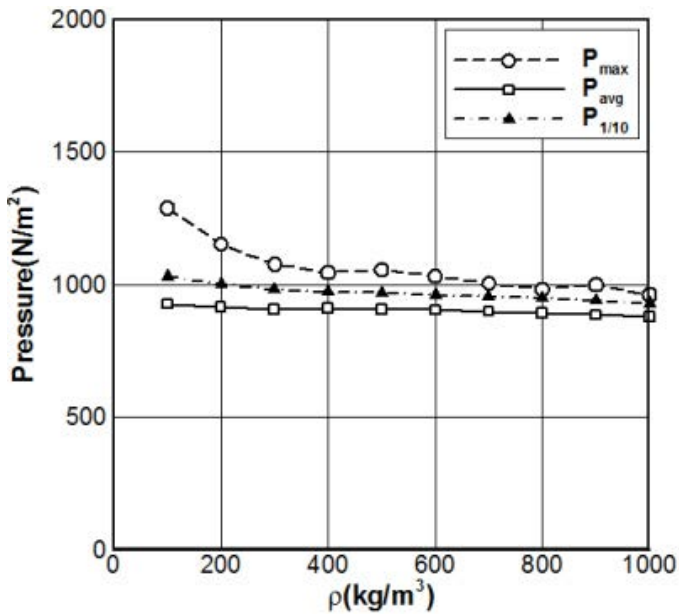


Figure 18: Results of statistical analysis for peak pressure at T=1.5 (s) with various density of floater (filling ratio=40%).

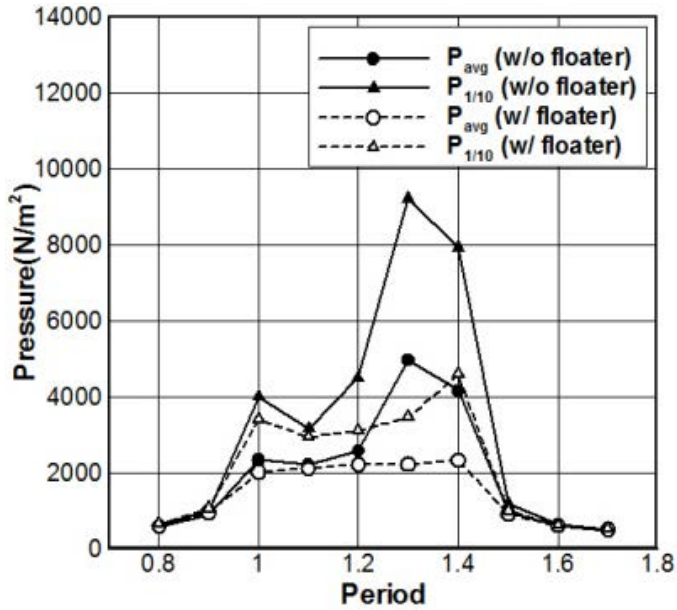


Figure 19: Comparison of peak pressure w/ and w/o floaters (filling ratio=40%).

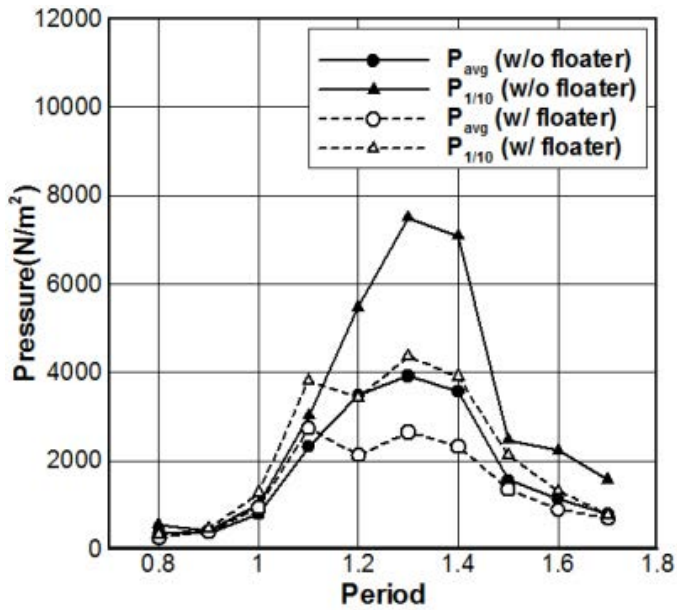


Figure 20: Comparison of pressure w/ and w/o floaters (filling ratio=20%).

their densities. It is also shown that the maximum impact loads can be effectively reduced by using properly chosen floater density. The reduction of impact loads in the presence of surface bubbles and foams may be related to the observed phenomenon although other factors like bubble compressibility may also play a role.

References

- Dalrymple, R.A.; Rogers B.D.** (2006) : Numerical modeling of water waves with the SPH method. *Coastal Engrg.* vol. 53, no. 2–3, pp. 141–147.
- Gingold, T.A.; Monaghan, J.J.** (1977) : Smoothed particle hydrodynamics: theory and application to non-spherical stars. *Mon. Not. R. Astron. Soc.* vol. 181, pp. 375–389.
- Gotoh, H.** (2009) : Lagrangian particle method as advanced technology for numerical wave flume. *Int. J. Offshore Polar Engrg.*, vol. 19, pp. 161–167.
- Hirt, C.W.; Nichols, B.D.** (1981) : Volume of fluid (VOF) method for the dynamics of free boundaries. *J. Comput. Phys.* vol. 39, pp. 201–225.
- Hwang, S.-C.; Lee, B.-H.; Park, J.-C.; Sung, H.-G.** (2010) : Particle-based Simulation for sloshing in a rectangular tank. *Korean Soc. Ocean Engrg.* vol. 24. no. 2, pp. 20–27 (in Korean).
- Idelsohn, S.R.; Onate, E.; Del Pin, F.** (2004) : The particle finite element method: a powerful tool to solve incompressible flows with free-surfaces and breaking waves. *Int. J. Numer. Methods Engrg.*, vol. 61, pp. 964–989.
- Khayyer, A.; Gotoh, H.** (2009) : Modified moving particle semi-implicit methods for the prediction of 2D wave impact pressure. *Coastal Engrg.* vol. 56, pp. 419–440.
- Khayyer, A.; Gotoh, H.** (2011) : Enhancement of stability and accuracy of the moving particle semi-implicit method. *Journal of Computational Physics.* vol. 230, pp. 3093–3118.
- Kim, Y.; Kim, S.-Y.; Kim, K.-H.; Jeon, S.-E.; Seo, Y.-S.; Park, J.-J.; Hwang-Bo, S.-M.; Lee, Y.-J.** (2011) : Model-Scale Sloshing Tests for an Anti-Sloshing Floating Blanket System. Proceedings of the ISOPE-2011, Hawaii, USA.
- Kishev, Z.; Hu, C.; Kashiwagi, M.** (2006) : Numerical simulation of violent sloshing by a CIP-based method. *J. Mar. Sci. Techol.*, vol. 11, pp. 111–122.
- Koshizuka, S.; Oka, Y.** (1996) : Moving-particle semi-implicit method for fragmentation of incompressible fluid. *Numer. Sci. Engrg.* vol. 123, pp. 421–434.
- Lamb, H.** (1932) : *Hydrodynamics*, Cambridge University Press, UK.
- Lee, B.-H.; Park, J.-C.; Kim, M.-H.; Hwang, S.-C.** (2011) : Step-by-step im-

provement of MPS method in simulating violent free-surface motions and impact-loads. *Comput. Methods Appl. Mech. Engrg.*, vol. 200, pp. 1113-1125.

Miyata, H.; Park, J.-C. (1995) : Ch. 5 wave breaking simulation, in: M. Rahman (Ed.), Potential Flow of Fluids. *Computational Mechanics Publications*, UK, pp. 149–176.

Monaghan, J.J.(1988) : An introduction to SPH. *Comput. Phys. Commun.*, vol. 48, pp. 89–99.

Sueyoshi, M.; Naito, S. (2003) : A numerical study of violent free surface problems with particle method for marine engineering. 8th Proceedings of the Numerical Ship Hydrodynamics, pp. 330–339.

Sussman, M.; Smereka, P.; Osher, S. (1994) : A level set approach for computing solutions to incompressible two-phase flow. *J. Comput. Phys.*, vol. 114, pp. 272–280.

Toyota, E.; Akimoto, H.; Kubo, S. (2005) : A particle method with variable spatial resolution for incompressible flows. 19th Japan Society of Fluid Mechanics, A9-2.